JOURNAL OF MATERIALS SCIENCE 30 (1995) 4628–4636

Numerical analysis for micropyretic synthesis of NiAl intermetallic compound

H. P. LI, J. A. SEKHAR
International Center for Micropyretics, Department of Materials Science and Engineering, P.O. Box 210012, University of Cincinnati, Cincinnati, OH 45221, USA

A numerical investigation of the micropyretic synthesis response parameters of the Ni–Al stoichiometric compound was undertaken. The influence of the enthalpy of the combustion reaction, Q, activation energy, E, amount of diluent, pre-exponential factor, K_0, and initial temperature T_0, on the combustion velocity, temperature, and mode was studied. The porosity of the unreacted compact, which is related to the initial compaction pressure, was considered in the calculation. It was found that the change in porosity significantly affects the thermal conductivity and the length of the pre-heat zone as also do the temperature patterns and propagation velocities. The combustion front was noted to be extinguished if the temperature in the reaction zone became lower than the melting point of the aluminium phase. This result was obtained simply by considering the changes in the thermal conductivity after the melting of aluminium without having to invoke any changes in the rate of reaction after the melting. A comparison of the numerical data with the experimental and analytical results was also made.

Nomenclature

A, B	Constants
D_0	Reference diffusion coefficient
E	Activation energy (J kg^{-1})
H	Enthalpy (J kg^{-1})
K^*	Thermal conductivity (J m^{-1} s^{-1} K^{-1})
K_0	Pre-exponential factor (s^{-1})
l_r	Length of the reaction zone
l_p	Length of the pre-heat zone
M_{FC}	Molar fraction of diluent present at any η
Q	Heat of reaction (J kg^{-1})
r	Diameter of the non-melting reactants
R	Universal gas constant (J kg^{-1} K^{-1})
T	Temperature (K)
T_c	Combustion temperature (K)
T_0	Initial temperature of the unreacted compact (K)
V	Propagation velocity (m s^{-1})
Z	Dimensional coordinate (m)
t	Dimensional time (s)
ρ	Density (kg m^{-3})
η	Volume fraction of reacted product
ϕ	Dimensionless enthalpy
ε_1	Specific error = 10^{-6}
ε_2	Specific error = 10^{-3}

Subscripts

U	Unreacted reactants
R	Reacted product

1. Introduction

Micropyretic/combustion synthesis [1–19] is a novel material processing in which the synthesis of compounds and composites is accomplished by the propagation of a combustion front through the sample. The heat to propagate the combustion front is obtained from the heat of formation of the synthesized compound. The unreacted portion in front of the combustion front is heated by this heat, undergoes synthesis thus allowing the combustion front to propagate, and causes further reaction and synthesis. Exothermic reaction processing circumvents difficulties associated with conventional methods of time and energy-intensive sinter processing and is being extensively studied for the synthesis of ceramic and intermetallic compounds [1–19]. The parameters which impact the velocity and temperature of self-propagating micropyretic synthesis are the heat of the combustion reaction, Q, the activation energy, E, the pre-exponential factor, K_0, thermal conductivity, K^*, and initial temperature, T_0. The propagation velocity and combustion temperature are the measurable processing response parameters for the design of micropyretically synthesized parts [11].

Various numerical studies for the combustion temperature and the velocity variation (called the response parameters) during micropyretic synthesis have been reported earlier [1, 2, 14]. Lakshmikantha *et al.* [1] developed a numerical method of solving for the micropyretic synthesis problem including

0022–2461

provisions for the solidification of the product. A systematic study of the influence of the initial processing parameters on the propagation velocity and combustion temperature during the micropyretic synthesis was reported for the Ti–C system [1]. A detailed investigation of the influence of the diluent and porosity in the TiB_2 and TiC systems was also carried out [2]. These numerical results, obtained by considering different values of porosities and diluents in the reactants, showed that the combustion temperature and propagation velocity were strongly dependent on the initial processing parameters. In addition, a numerical model for multidimensional analysis of micropyretic synthesis has also been developed [14].

Intermetallic compounds containing aluminium have attractive combinations of low density, high-temperature strength, good corrosion and oxidation resistance, relatively low cost, and high thermal stability. Among these aluminides, NiAl possesses ideal mechanical and physical properties and is considered to be a candidate for high-temperature applications [20]. Nickel aluminide is made easily in net shape by micropyretic synthesis [8, 11]. In this work the synthesis of NiAl was studied numerically. The influence of the heat of the exothermic reaction, Q, the activation energy, E, the amount of diluent, the pre-exponential factor, K_0, and the initial temperature, T_0, on the temperature/distance profiles for self-propagating micropyretic synthesis, was studied, following the numerical methods developed earlier [1, 2]. Further, the effect of the porosity, which is related to the initial compaction pressure, was also considered in the calculation. It was found that the change of the porosity significantly affects the thermal conductivity and the length of reaction/pre-heat zone, and further influences the temperature patterns and propagation velocities. Finally, a comparison of the numerical data, analytically determined values, and experimental results for NiAl [8, 11] is presented.

2. Numerical model

2.1. Mathematical formulation

The energy equation for transient heat conduction, which includes the source term, containing the heat release on account of the exothermic micropyretic reaction is given by [1, 2]

$$\rho\frac{\partial H}{\partial t} = \left[\partial\left(K^*\frac{\partial T}{\partial Z}\right)\Big/\partial Z\right] + \rho Q K_o \times (1 - M_{FC})(1 - \eta)\exp\left(\frac{-E}{RT}\right) \quad (1)$$

In the equation, the first term on the right-hand side is the conduction heat transfer term. The second term gives the heat release on account of the exothermic micropyretic reaction. The unreacted fraction of the specimen $(1 - \eta)$, which contributes to the heat of reaction from the micropyretic synthesis, is considered in the energy source term of Equation 1.

The porosity of the reactants and product which affects the thermal conductivity and density is also considered in the calculation. For the calculations, the thermal conductivity and density of the reactants and product with the porosity can be expressed as

thermal conductivity:

$$K^*_{\text{porosity}} = K^*_{\text{without porosity}}(1 - P)/[1 + (P/2)] \quad (2)$$

density:

$$\rho_{\text{porosity}} = \rho_{\text{without porosity}}(1 - P) \quad (3)$$

where P is the porosity of the reactants or product. The effect of melting of reactants, nickel and aluminium and product, NiAl, is also included in the calculation procedure.

2.2. Numerical procedure

An enthalpy–temperature method coupled with Guass Sidel iteration procedure was used to solve the equations. First, the temperatures and enthalpies at all nodes are initialized by using the proper initial and boundary conditions. The initial conditions assumed are: (1) at the first node, at time $t \geq 0$, the temperature is taken to be the adiabatic combustion temperature, i.e. $T = T_c$ and $\eta = 1$. It has been reported that the chosen temperature value at the first node will not influence the numerical results, except at the initial stages of the propagation [16]; (2) at the other nodes, at time $t = 0$, the temperatures are taken to be the same as the substrate temperature, i.e. $T = T_0$ and $\eta = 0$.

The total length of the sample and the number of nodes taken for the calculation are 0.01 m and 1201, respectively. The time step used ranges from 2.5×10^{-4} to 2.5×10^{-2} s, depending on the chosen pre-exponential values, K_0. The convergence criterion used to ascertain whether the reacted fraction, η, and enthalpy, ϕ, at each time level converges or not, is from the relative error criterion, i.e. absolute values of the $[(\eta^{m+1} - \eta^m/\eta^{m+1})]$ and $[(\phi^{m+1} - \phi^m)/\phi^{m+1}]$ for all nodes, must be less or equal to ε_1 and ε_2, respectively. The symbols $(m + 1)$ and m stand for the current iteration and previous iteration, respectively. The values of ε_1 and ε_2 are taken to be 10^{-6} and 10^{-3} in this article, respectively. Once the convergence criterion is met, the enthalpy and reacted fraction of the last iteration in a time step are considered as the corresponding final values at each node. The calculations are performed for various times depending upon the problem.

In the calculation, the melting point for the NiAl stoichiometric composition is taken to be 1912 K [21], and the exothermic heat and the activation energy of micropyretically synthesized NiAl intermetallic compound are taken to be 118.5 [21] and 139 kJ mol^{-1} [22], respectively. The various thermophysical/chemical parameters, including the thermal conductivities, the densities, and the heat capacities, are assumed to be independent of temperature but they are different in each state. The average values of these parameters vary as the reaction proceeds, depending upon the degree of reaction. The parameter values used in the calculation are shown in Tables I–III [21, 23, 24].

TABLE I The thermophysical/chemical parameters for the reactants and product at 300 K

Thermophysical/chemical parameters	Al	Ni	NiAl
Specific heat of unreacted product at 300 K ($J\,kg^{-1}K^{-1}$)	902 [21]	445 [21]	537 [21]
Specific heat of reacted solid product at high temperature ($J\,kg^{-1}K^{-1}$)	1100 [21]	547 [21]	640 [21]
Specific heat of reacted liquid product ($J\,kg^{-1}K^{-1}$)	1178 [21]	735 [21]	831 [21]
Thermal conductivity of unreacted product at 300 K ($J\,m^{-1}s^{-1}K^{-1}$)	238 [24]	88.5 [24]	75 [23]
Thermal conductivity of reacted solid product at high temperature ($J\,m^{-1}s^{-1}K^{-1}$)	238 [24]	58 [23]	65 [23]
Thermal conductivity of reacted liquid product ($J\,m^{-1}s^{-1}K^{-1}$)	100 [24]	53 [23]	55 [23]
Density of unreacted product at 300 K ($kg\,m^{-3}$)	2700 [24]	8900 [24]	6050 [23]
Density of reacted solid product at high temperature ($kg\,m^{-3}$)	2700 [24]	8900 [24]	6050 [23]
Density of reacted liquid proudct ($kg\,m^{-3}$)	2385 [24]	7905 [24]	5950 [24]

TABLE II The thermophysical/chemical parameters for the reactants and product at 520 K

Thermophysical/chemical parameters	Al	Ni	NiAl
Specific heat of unreacted product at 520 K ($J\,kg^{-1}K^{-1}$)	1006 [21]	539 [21]	573 [21]
Specific heat of reacted solid product at high temperature ($J\,kg^{-1}K^{-1}$)	1100 [21]	547 [21]	640 [21]
Specific heat of reacted liquid product ($J\,kg^{-1}K^{-1}$)	1178 [21]	735 [21]	831 [21]
Thermal conductivity of unreacted product at 520 K ($J\,m^{-1}s^{-1}K^{-1}$)	238 [24]	80 [24]	72 [24]
Thermal conductivity of reacted solid product at highl temperature ($J\,m^{-1}s^{-1}K^{-1}$)	238 [24]	58 [23]	65 [23]
Thermal conductivity of reacted liquid proudct ($J\,m^{-1}s^{-1}K^{-1}$)	100 [24]	53 [23]	55 [23]
Density of unreacted product at 520 K ($kg\,m^{-3}$)	2700 [24]	8900 [24]	6050 [23]
Density of reacted solid product at high temperature ($kg\,m^{-3}$)	2700 [24]	8900 [24]	6050 [23]
Density of reacted liquid proudct ($kg\,m^{-3}$)	2385 [24]	7905 [24]	5950 [24]

TABLE III The thermophysical/chemical parameters for the reactants and product at 670 K

Thermophysical/chemical parameters	Al	Ni	NiAl
Specific heat of unreacted product at 670 K ($J\,kg^{-1}K^{-1}$)	1073 [21]	542 [21]	597 [21]
Specific heat of reacted solid product at high temperature ($J\,kg^{-1}K^{-1}$)	1126 [21]	547 [21]	640 [21]
Specific heat of reacted liquid product ($J\,kg^{-1}K^{-1}$)	1178 [21]	735 [21]	831 [21]
Thermal conductivity of unreacted product at 670 K ($J\,m^{-1}s^{-1}K^{-1}$)	238 [24]	70 [24]	70 [24]
Thermal conductivity of reacted solid product at high temperature ($J\,m^{-1}s^{-1}K^{-1}$)	238 [24]	58 [23]	65 [23]
Thermal conductivity of reacted liquid product ($J\,m^{-1}s^{-1}K^{-1}$)	100 [24]	53 [23]	55 [23]
Density of unreacted product at 670 K ($kg\,m^{-3}$)	2700 [24]	8900 [24]	6050 [23]
Density of reacted solid product at high temperature ($kg\,m^{-3}$)	2700 [24]	8900 [24]	6050 [23]
Density of reacted liquid proudct ($kg\,m^{-3}$)	2385 [24]	7905 [24]	5950 [24]

3. Influence of combustion parameters on combustion temperature and velocity

3.1. Initial temperature

Because the propagation of the combustion occurs due to the released energy from the exothermic micropyretic reaction, an understanding of the enthalpy change during the reaction can be used to predict theoretically the adiabatic combustion temperature [25]. Fig. 1 shows the plot of the adiabatic combustion temperature and the melted fraction of product phase with the initial temperature of the unreacted compact. The values of the enthalpy and the heat capacity for calculating the adiabatic combustion temperature are taken from Bovin *et al.* [21]. The adiabatic combustion temperature is calculated to be 1912 K, which is the same as the melting point of the NiAl product, when the initial temperature is taken to be the standard room temperature (300 K). Up to an initial temperature of 920 K, the adiabatic combustion temperature remains constant with the only change being the increase in the molar melted fraction of the product phase from 42% to 100%. Above 920 K initial temperature, the adiabatic combustion temperature begins to increase with the initial temperature, however, it is not linearly proportional to the initial temperature, as noted from Fig. 1. This is because the absolute values of the enthalpy of reactants are significantly changed at the melting temperatures of reactants on account of the latent heat. The melting

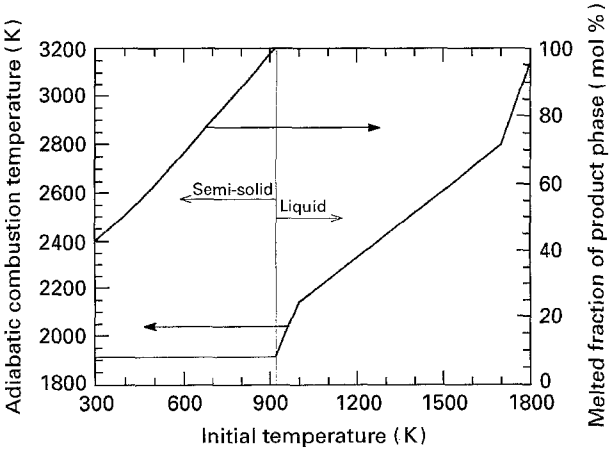

Figure 1 A plot of adiabatic combustion temperature and the melted molar fraction of product phase with the initial temperature.

points of the aluminium phase and the nickel phase are 933 and 1726 K, respectively, thus the slopes are noted to change at these temperatures.

Fig. 2 shows the typical temperature profiles for the various initial temperatures: 300, 520, and 670 K. Note the small instabilities which set in as the initial temperature is increased. From the intervals of time and distance, the average propagation velocity can be calculated. Normally an increase in the initial temperature increases the enthalpy in the system and further increases both combustion temperature and propagation velocity. However, note from Fig. 2 that the propagation velocity is increased but the combustion temperature remains constant when the initial temperature is increased. As described in the previous paragraph, an increase in the enthalpy on account of increasing the initial temperature, is only used by the system to increase the melted fraction of the product phase. Thus, the temperature is noted to remain constant even though the enthalpy and the propagation velocity are increased.

3.2. Pre-exponential factor

A change in the pre-exponential factor, or frequency factor, K_0, is known to influence the velocity of the front propagation [1–3]. It has been reported that, depending on the value of K_0, the effect of the thermal conductivity may increase or decrease the velocity of the propagation [1]. The K_0 value is reported to be proportional to D_0/r^2, where D_0 is the reference diffusion coefficient and r is the diameter of the non-melting reactants [2]. Fig. 3 shows a plot of the average propagation velocity at various K_0 values in the Ni–Al system. The propagation velocity is noted to increase as K_0 is increased; however, the combustion temperature remains constant with an increase in K_0.

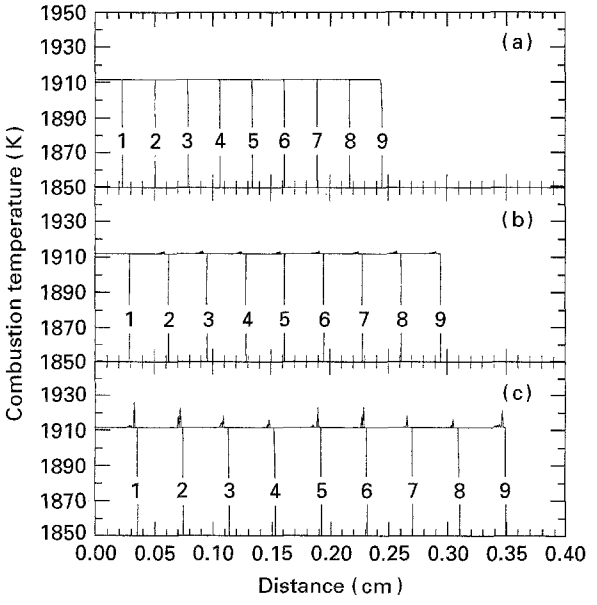

Figure 2 A plot of the combustion front temperature at various times along the length of the specimen. The initial temperatures, T_0 used are (a) 300 K, (b) 520 K, and (c) 670 K. In the calculation, $E = 139$ kJ mol^{-1}, $Q = 118.5$ kJ mol^{-1}, and $K_0 = 8 \times 10^8$ s^{-1}. The time interval between two consecutive time steps is 0.0005 s.

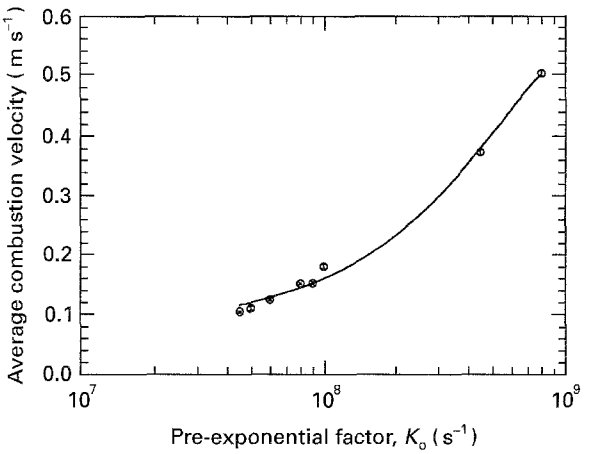

Figure 3 A plot of the average combustion velocity with the pre-exponential factor, K_0, of the samples with 50% porosity. The experimental value for the propagation velocity of the specimen, which contains 50% reactant porosity and 30% final porosity, is 0.119 m s^{-1}. $Q = 118.5$ kJ mol^{-1}, $E = 139.0$ kJ mol^{-1}, $T_0 = 300$ K.

An increase in the K_0 value is equivalent to decreasing the particle size of the reactant or increasing the reference diffusion coefficient, and further increases the kinetics of the reaction. Hence, an increase in the K_0 value is found to increase the propagation velocity.

3.3. Activation energy and exothermic heat

The activation energy, E, has a pronounced effect on the propagation velocity while not influencing the combustion temperature, as shown in Fig. 4 and [1]. A decrease in the activation energy increases the kinetics of the reaction, and further increases the propagation velocity. Note from Fig. 4 that an increase in the activation energy beyond 146 kJ mol^{-1} leads to extinction, and a decrease below 130 kJ mol^{-1} results in an exponential increase in the velocity. The propagation velocity is quickly increased to 742 m s^{-1} when the activation energy is reduced to 40 kJ mol^{-1}. The combustion temperature, on the other hand, is relatively insensitive to a change in activation energy and is slightly below 1912 K. The activation energy may also affect the nature of the propagation. It is noted

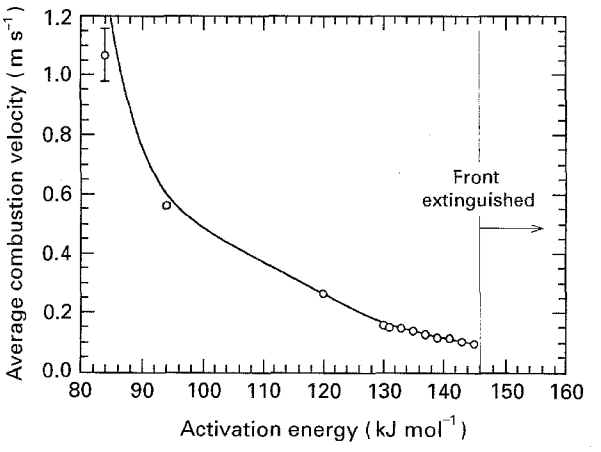

Figure 4 The variation of the average combustion velocity with the activation energy, E. $K_0 = 4.5 \times 10^7$ s^{-1}, $T_0 = 300$ K, $Q = 118.5$ kJ mol^{-1}.

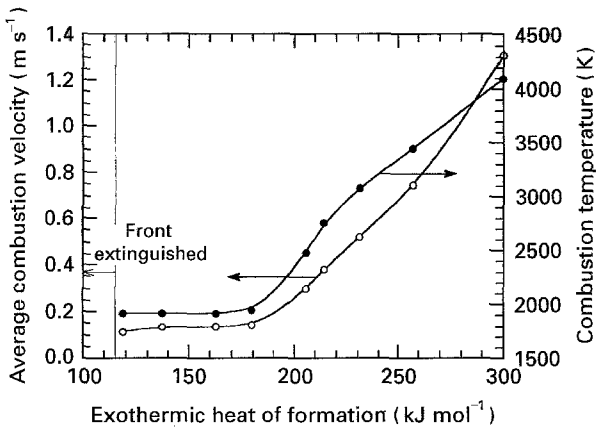

Figure 5 The variation of the average combustion velocity with the reaction enthalpy, Q. $K_0 = 4.5 \times 10^7\ s^{-1}$, $T_0 = 300$ K, $E = 139\ kJ\ mol^{-1}$.

that in the Ni–Al system when the activation energy is increased to a higher level, an unstable irregular temperature pattern is observed.

A plot of the exothermic heat of the reaction, Q, and combustion temperature/velocity is shown in Fig. 5. For simplifying the calculation, the adiabatic combustion temperature at the first node is still assumed to be 1912 K, even though the exothermic heat is increased. As described above, such an assumption will only affect the initial propagation state [16]. These initial irregular propagations are not be considered in calculating the average propagation velocity. Note from Fig. 5 that a decrease in the exothermic heat decreases both the combustion temperature and propagation velocity. When the exothermic heat is reduced to 160 kJ mol^{-1}, the combustion temperature remains constant which is close to the melting point of the NiAl product (1912 K) and the propagation velocity is noted to decrease slightly. The combustion front ceases to propagate with a decrease in the exothermic heat to 115 kJ mol^{-1} (Fig. 5).

3.4. Diluent

The end product of the micropyretic reaction, NiAl, is also chosen to be the diluent for such calculations. An increase in the amount of the diluent decreases the exothermic energy, hence, the combustion temperature and velocity are expected to decrease with the addition of the diluent. Fig. 6 shows that an increase in the diluent from 5 at % to 15 at % reduces combustion temperature from 1895 K to 1862 K, and decreases propagation velocity from 0.167 m s^{-1} to 0.146 m s^{-1}. A further increase of the diluent up to 25 at % decreases the combustion temperature to 1829 K and causes the combustion front to be extinguished (Fig. 6c).

4. Reaction zone and pre-heat zone

Reaction and pre-heat zones are associated with the combustion front propagation [1]. Figs 7 and 8 show the typical combustion profiles in the reaction/pre-heat zone of the specimen with 30% initial porosity and 30% product porosity. The combustion front

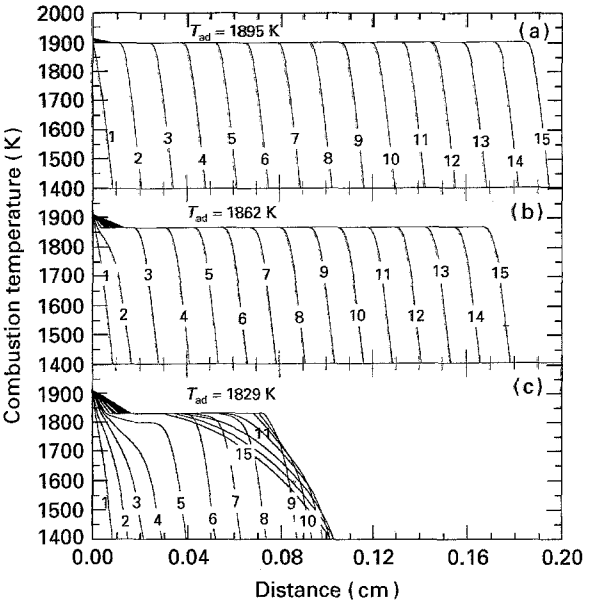

Figure 6 A plot of the combustion front temperature at various times along the length of the specimen. The amounts of the diluent (NiAl) used are (a) 5 at %, (b) 15 at %, and (c) 25 at %. In the calculation, T_0 is taken to be 300 K, $E = 139\ kJ\ mol^{-1}$, $Q = 118.5\ kJ\ mol^{-1}$, and K_0 is $4.5 \times 10^7\ s^{-1}$. The time interval between two consecutive time steps is 0.0011 s.

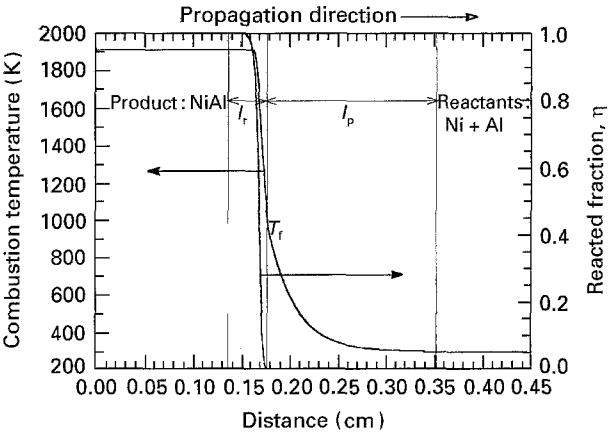

Figure 7 The temperature and reacted fraction profiles along the specimen with 30% porosity at time step of 0.0164 s.

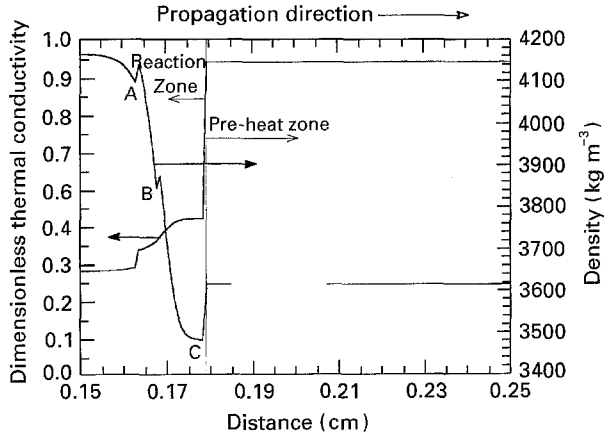

Figure 8 The dimensionless thermal conductivity and density profiles along the specimen with 30% porosity at time step of 0.0164 s.

propagates from the left to the right. Fig. 7 shows the combustion temperature and the reacted fraction, η, variation along the specimen at the time step of 0.0164 s. For the time shown, the combustion front propagates to the position ~ 0.15 cm. During the passage of the combustion front, the reactants, nickel and aluminium, react to form the NiAl stoichiometric product. Depending on the temperature and reacted fraction distributions, the reaction zone and preheat zone can be characterized between the reactants and product. The length of the reaction zone, l_r, is defined as $0.0005 \leq \eta < 1$ and the length of the pre-heat zone, l_p, starts from the end of the reaction zone until the position where the combustion temperature reaches the original substrate temperature. In the pre-heat zone, the reacted fraction approaches zero and the density and thermal conductivity remain constant.

Fig. 8 shows the plot of the dimensionless thermal conductivity and density along the specimen. The density is strongly influenced by the phase change of the reactants and product. Therefore, the density is noted to change sharply at temperatures where phase transformations take place. For instance, the density is increased at the position B which corresponds to the melting point of the nickel phase. The density of the nickel solid phase is higher than that of the nickel liquid phase. Therefore, the density at the position B is noted to be higher on account of the solidification of the molten nickel. On account of the increase in the percentage of the reactants with the distance in the reaction zone, the density continuously drops until the molten aluminium solidifies, as shown in Fig. 8. At position C, the density is increased again on account of the molten aluminium solidifying. Also shown in Fig. 8 is the variation of the dimensionless thermal conductivity with the distance in the reaction zone. It is noted that the phase transformation causes the abrupt change of the density in the reaction zone, and further influences the dimensionless thermal conductivity distribution.

Note from Fig. 7 that when the combustion temperature in the reaction zone is decreased to ~ 930 K, which is close to the melting point of the aluminium phase (933 K), no reaction occurs (i.e. $\eta \sim 0$) and the pre-heat zone starts. An experiment reported earlier [19] also indicates that the combustion starts at the melting point of the aluminium phase. Thus both experiments, i.e. our numerical experiment and the real experiment, show that the combustion will not take place until the aluminium phase is molten. In other words, the temperature in the reaction zone must be higher than the melting point of the aluminium phase (933 K) to propagate the combustion front.

In the numerical calculation, the values which are influenced by the melting of the aluminium phase are density, heat capacity, and thermal conductivity of the reactant aluminium. The values of the density and heat capacity are noted only to slightly change after the solidification of the aluminium phase, but the thermal conductivity is significantly enhanced when the molten aluminium solidifies. A plot of the different thermal conductivities of the aluminium phase with the propagation velocity is shown in Fig. 9. When the thermal conductivity is increased to a high level, more heat is conducted to the pre-heat zone and the heat loss from the reaction zone increases. Thus, the propagation velocity is noted to decrease with an increase in the thermal conductivity from 100 J m^{-1} s^{-1} K^{-1} to 280 J m^{-1} s^{-1} K^{-1}. A further increase in the thermal conductivity to 350 J m^{-1} s^{-1} K^{-1} results in the stop of the combustion front. This explains why propagation ceases when the aluminium is solidified. Note that this result is not argued on the basis of a better spread and improved contact efficiency (i.e. higher K_0) after the aluminium melts. An improved contact efficiency increases the K_0 value and further aids to propagate the combustion front. It is found that for the extinguished combustion front which has higher thermal conductivity (350 J m^{-1} s^{-1} K^{-1}), an increase in K_0 from the value (5×10^7 s^{-1}) of no propagation to 1×10^8 s^{-1} causes the combustion front to propagate.

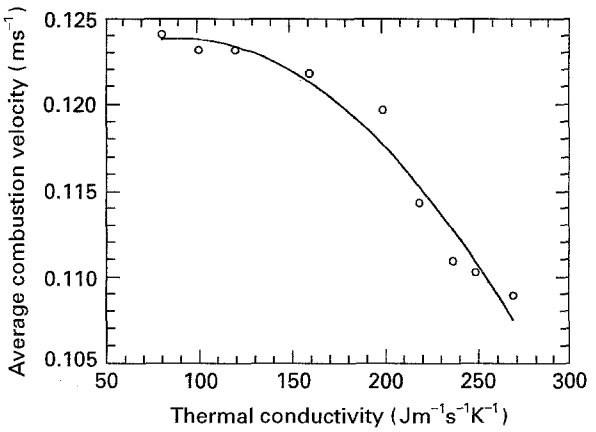

Figure 9 A plot of the average combustion velocity for the different thermal conductivities of the reactant aluminium phase.

The length of the reaction/pre-heat zone may have a pronounced influence on the nature and velocity of the combustion front. A significant increase in the length of the pre-heat zone, l_p, increases the heat loss from the combustion front. The velocity is thus decreased and the combustion front becomes more unstable. At the extreme case, the heat loss is significantly enhanced and the combustion front may not propagate [10]. Fig. 10 shows that there is a correlation between the length of the pre-heat zone and propagation velocity. An increase in the length of the pre-heat zone decreases the propagation velocity. The combustion front is noted to be extinguished when the length of pre-heat zone exceeds ~ 2.3 mm.

5. Porosity

It has been reported that the porosity has a dramatic effect on the mechanical properties of the product [7]. The porosity also influences the thermal conductivity and density of the unreacted compact and further changes the temperature and velocity of the combustion front. In many instances, the combustion front may not propagate at all as is found when the thermal conductivity is significantly increased or

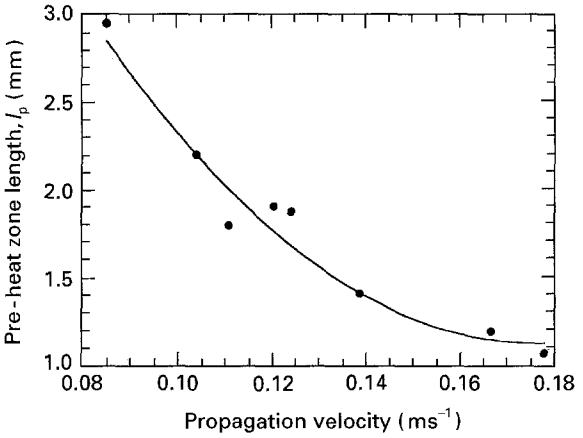

Figure 10 Plots of the length of pre-heat zone, l_p, with the average propagation velocity of the combustion front.

decreased [1]. Therefore, it is important to consider the influence of porosity in the numerical investigation.

The effect of the porosity on the propagation velocity is shown in Fig. 11. It is noted that initially the propagation velocity slightly increases and then decreases with an increase in the porosity. In this calculation, the porosities of the reactants and product are considered to be the same. The change in the porosity significantly influences the thermal conductivity as noted in Fig. 12a. Thus, the temperature distribution and the length of the reaction/pre-heat zones as well as the propagation velocity are further affected by the porosity. In Fig. 12, the coordinate origin is referred to the start of the reaction zone, in order to compare the lengths of the reaction zone at different porosity. Initially with a decrease in the porosity from 50% to 10%, the particle interfacial contacts increase, thus, the thermal conductivity and the efficiency of the heat transfer to the pre-heat zone are enhanced. The lengths of the reaction zone, l_r, subsequently increase. The heat transfer accelerates to the next region and helps the propagation velocity to increase. Therefore, the specimen with 10% porosity propagates faster than those with 30% and 50% porosity, as noted in Figs 11 and 12. However, as porosity is continuously

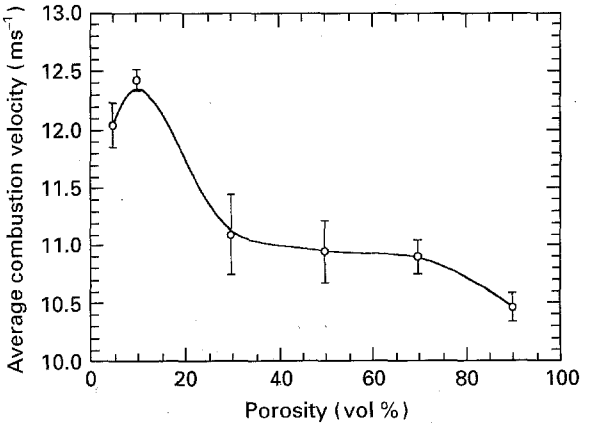

Figure 11 A plot of the average combustion velocity for the various porosities of the reactants and product. The initial temperature is taken as 300 K. $K_0 = 5 \times 10^7$ s^{-1}, $Q = 118.5$ kJ mol^{-1}, $E = 139.0$ kJ mol^{-1}, $T_0 = 300$ K.

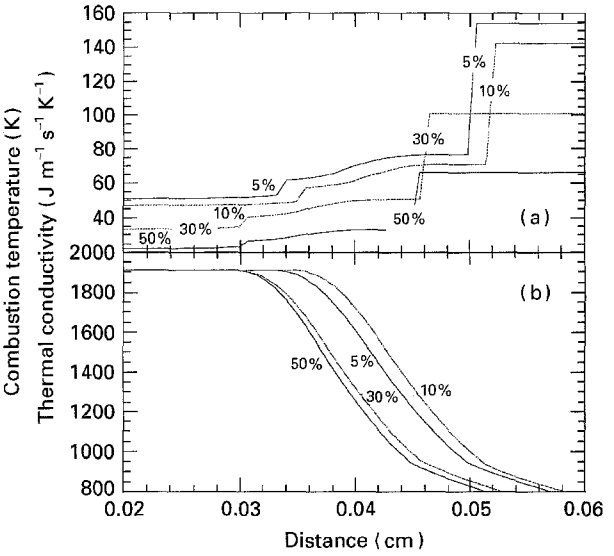

Figure 12 (a) The thermal conductivity and (b) the temperature profiles of the specimens with different porosities in the reaction and pre-heat zones. The distance shown in the figure is taken from the start of the reaction zone. The time steps for all the profiles are all the same, 0.0164 s.

decreased to a lower level, 5%, the propagation velocity starts to decrease. As porosity is continuously decreased, the contact areas increase significantly, resulting in an increase in the effective thermal conductivity of the compact. The increased rate of heat transfer from the reaction zone to the pre-heat zone continuously increases the length of the pre-heat zone, but decreases the length of the reaction zone. A significant increase in the length of pre-heat zone causes more heat loss, which is necessary in the reaction region to maintain a steady state propagation of the combustion wave. Hence, note from Fig. 12 that the propagation velocity of the specimen with 5% porosity is slower than that with 10% porosity. In the extreme case, the lower porosity may create instabilities in the combustion wave and alter the mode of the combustion [1, 2, 6].

6. Comparison with analytical models and experimental results

Table IV shows the comparisons among the numerical results, the analytically determined values, and the experimental data [8, 11]. In the numerical calculation, the pre-exponential factor, K_0 (5×10^7), is obtained by matching the experimental and numerical values from Fig. 3. The value of the pre-exponential factor is assumed to remain constant with respect to the change of the compaction pressure and initial temperature (from 300 K to 670 K). The analytical calculation for the propagation velocity of micropyretic synthesis has been reported elsewhere [18]. The propagation velocity of the combustion front is expressed as follows [18]

$$V^2 = \left[1 \Big/ f\left(\frac{\rho Q}{K^*}\right)\right]\left(\frac{K_0 R T_C^2}{2E}\right)\exp\left(\frac{-E}{RT_C}\right) \quad (4a)$$

TABLE IV The comparison of the numerical data with the experimental values [8, 11] and analytical results under different processing conditions

Initial temperature (K)[a]	Initial porosity(%)	final porosity(%)	Experimental values ($m\,s^{-1}$)	Analytical result ($m\,s^{-1}$)	Numerical data ($m\,s^{-1}$)
300	39	32	0.119 ± 0.006	0.127	0.110
520	39	31	0.162 ± 0.008	0.151	0.137
670	39	28	0.174 ± 0.010	0.180	0.171
Compaction pressure (MPa)[b]					
34.5	51	37	0.070 ± 0.007	0.120	0.107
103.4	39	32	0.119 ± 0.006	0.127	0.110
172	31	21	0.122 ± 0.011	0.129	0.114
241.3	25	38	0.111 ± 0.012	0.138	0.115

[a]These specimens were compacted at 103.4 MPa (15 000 p.s.i).
[b]These specimens were ignited at 300 K.

where

$$f\left(\frac{\rho Q}{K^*}\right) = A + B \ln\left(\frac{K_R^*}{K_U^*}\right) \tag{4b}$$

with

$$A = \left[\frac{Q(\rho_R - \rho_U)K_U^*}{(2K_R^* - K_U^*)^2}\right] - \frac{Q(\rho_R - 3\rho_U)}{4(K_R^* - K_U^*)} \tag{4c}$$

$$B = \left[\frac{Q\rho_U K_U^*}{(K_R^* - K_U^*)^2}\right] - \left[\frac{Q(\rho_R - \rho_U)K_U^{*2}}{2(K_R^* - K_U^*)^3}\right] + \left(\frac{\bar{C}_p(T_C - T_0)}{(1 - M_{FC})(K_R^* - K_U^*)}\right) \tag{4d}$$

and

$$\bar{C}_p = \frac{1}{2}[C_{p^R}\rho_U + C_{p^U}\rho_R] + \frac{1}{3}[(C_{pR} - C_{pU})(\rho_R - \rho_U)] \tag{4e}$$

The various parameters used in the analytical calculation and pre-exponential factor are the same as those used in the numerical procedure. The porosity is also considered in the analytical calculations (Equations 2 and 3). The porosity of the reactants and product for each processing condition is taken from the experimental results, as also shown in Table IV. Note from the Table IV that as the initial temperature of the unreacted compact increases, the experimental, analytical, and numerical results all increase. When the compaction pressure is changed, the agreement among the numerical predictions and analytically/experimentally determined numbers is noted to be close, except for the composition with the very low compaction pressure. A further lowering of the K_0 value of 3×10^7 is adequate to match the experimental values for the low compaction pressure experiments.

7. Conclusion

A numerical investigation for micropyretically synthesised NiAl compound has been studied. The variation of the combustion velocity and temperature with the initial temperature, T_0, pre-exponential factor, K_0, activation energy, E, exothermic heat, Q, diluent, and the porosity effect is reported. When the initial temperature is below 920 K, an increase in the initial temperature only increases the propagation velocity while the combustion temperature remains the same. Beyond 920 K, the combustion temperature and propagation velocity are both increased with the initial temperature. The propagation velocity increases when the pre-exponential factor is increased. The activation energy, E, has a pronounced effect on reducing the propagation velocity while not influencing the combustion temperature. However, an increase in the exothermic heat, Q, is noted to increase both the combustion temperature and propagation velocity. Extinction conditions are approached with decreasing Q and increasing E. The addition of the diluent decreases both the combustion temperature and propagation velocity. When the amount of the diluent exceeds 25 at %, the combustion front cannot propagate.

The initial temperature in the combustion experiment when propagation proceeds smoothly corresponds to the melting point of aluminium. This could be explained simply by considering thermal conductivity changes at the aluminium melting point. The reported results could not further test whether the increased contact efficiency obtained after the aluminium melted also had a significant influence on the propagation. The consideration of porosity, which is related to the initial compaction pressure, reveals that the propagation velocity at first increases then decreases with the increase in the porosity. A plot of the thermal conductivity and reacted fraction along the reaction and pre-heat zones shows the melting of the various phases influencing the combustion parameters. A comparison of the numerical results with the analytical and experimental values was also studied. The agreement between the numerical model predictions and the analytically/experimentally determined numbers is noted to be close, if the proper K_0 value is chosen.

Acknowledgement

This work was carried out for the Air Force Office of Scientific Research under grant AFOSR-F49620-93-1-0200 monitored by Dr Charles Ward.

References

1. M .G. LAKSHMIKANTHA, A. BHATTACHARYA and J. A. SEKHAR, *Metall. Trans.* **23A** (1992) 23.
2. M. G. LAKSHMIKANTHA and J. A. SEKHAR, *ibid.* **24A** (1993) 617.
3. A. G. MERZHANOV and B. I. KHAIKIN, *Prog. Energy Combust. Sci.* **14** (1988) 1.
4. A. G. MERZHANOV, in "Combustion and Plasma Synthesis of High-Temperature Materials", edited by Z. A. Munir and J. B. Holt (VCH, New York, NY, 1990) pp. 1–53.
5. Z. A. MUNIR, *Am. Ceram. Bull.* **34** (1988) 342.
6. R. W. RICE, *J. Mater. Sci.* **26** (1991) 6533.
7. H. P. LI, S. BHADURI and J. A. SEKHAR, *Metall. Trans* **23A** (1992) 251.
8. H. P. LI and J. A. SEKHAR, *Mater. Sci. Eng.* **A160** (1993) 221.
9. A. BOSE, B. H. RABIN and R. M. GERMAN, *Powder Metall. Int.* **20**(3) (1988) 25.
10. Z. A. MUNIR and U. ANSELMI-TAMBURINI, *Mater. Sci. Rep.* **3** (1989) 277.
11. H. P. LI and J. A. SEKHAR, in "Advanced Synthesis of Engineered Structural Materials", edited by J. J. Moore, E. J. Lavernia, and F. H. Froes (ASM International, Materials Park, OH, 1993) pp. 25–31.
12. J. A. SEKHAR, S. B. BHADURI, H. P. LI and N. S. CANARSLAN, US Pat. 5188678, 23 February 1993.
13. J. A. SEKHAR, A. K. BHATTACHARYA and H. P. LI, US Pat. 5110688 5 May 1992.
14. M. G. LAKSHMIKANTHA and J. A. SEKHAR, *J. Mater. Sci* **28** (1993) 6403.
15. K. G. SHKADINSKII, B. I. KHAIKIN and A. G. MERZHANOV, *Combust. Explos. Shock Waves* **7**(1) (1971) 15.
16. H. P. LI and J. A. SEKHAR, *J. Mater. Res.* **8** (1993) 2515.
17. C. NISHIMURA and C. T. LIU, *Acta. Metall. Mater.* **41** (1993) 113.
18. M. G. LAKSHMIKANTHA and J. A. SEKHAR, *J. Am. Ceram. Soc.* **77** (1994) 202.
19. H. P. LI and J. A. SEKHAR, submitted.
20. C. T. LIU and J. O. STEIGLER, *Science* **226** (1984) 636.
21. I. BARIN, O, KNACKE and O. KUBASCHEWSKI, "Thermochemical Properties of Inorganic Substances" (Springer, New York, NY, 1973) p. 489.
22. Y. S. NAIBORODENKO and V. I. ITIN, *Combust. Explos. Shock Waves* **11** (1975) 293.
23. D. R. LIDE, "CRC Handbook of Chemistry and Physics" (CRC, Boca Raton, IL, 1990).
24. E. A. BRANDES and G. B. BROOK, "Smithells Metals Reference Book" (1992).
25. J. A. RODRIGNES, V. C. PANDOLFELLI, W. J. BOTTAF, R. TOMASI, B. DERBY, R. STEVENS and R. J. BROOK, *J. Mater. Sci. Lett.* **10** (1991) 819.

Received 7 March 1994
and accepted 5 April 1995